SEISMIC RETROFIT OF A REINFORCED CONCRETE SCHOOL BUILDING USING DISSIPATIVE STEEL BRACES

M. Ferraioli*, A. Lavino*, G. Di Lauro and A. Mandara***

*Department of Civil Engineering, Design, Building and Environment
University of Campania 'Luigi Vanvitelli', Aversa (CE) – Italy
e-mails: massimiliano.ferraioli@unicampania.it, angelo.lavino@unicampania.it, alberto.mandara@unicampania.it

** Aires Ingegneria, Caserta – Italy
e-mail: dilauro@airesingegneria.it

Abstract. *The paper illustrates the seismic retrofit carried out on an existing school building located in Italy by means of dissipating steel braces. The preliminary investigations, the design project, the construction process and, eventually, the seismic response of the retrofitted building were presented. At first, the manuscript reports the comprehensive study on the seismic vulnerability of the existing reinforced concrete framed building. Many deficiencies consisting in improper detailing, poor quality of materials and inadequate ductility were found. Furthermore, the torsional effects in this plan irregular building due to the L-shape floor plans were evidenced. Then, the paper illustrates the displacement-based design procedure of supplemental energy dissipation devices for seismic retrofit. Both buckling-restrained axial dampers and steel hysteretic dampers were considered for seismic upgrading of the reinforced concrete frame building. The effectiveness and reliability of the adopted seismic retrofitting technique and design approach were finally investigated using comprehensive nonlinear static and dynamic analyses.*

1 INTRODUCTION

Many existing RC buildings were designed without earthquake-resistance requirements (pre-code structures) or following outdated structural codes and, thus, they may lack adequate seismic resistance. This is especially true for public buildings such as hospitals or schools, whose seismic resistance is of importance in view of the consequences associated with their collapse [1-2]. Often, low-rise RC school buildings have large windows with a long rectangular floor plan, thus creating a seismically weak direction along the internal corridor. Moreover, the seismic gap between adjacent buildings is not adequate to accommodate their relative motions, thus resulting in a significant seismic hazard of pounding during earthquake excitation. Finally, the torsion effect on plan irregular buildings [3-4] may considerably increase their seismic vulnerability. Thus, these buildings demand efficient retrofitting to ensure safety during and after earthquakes. One suitable seismic retrofit solution is the installation of dissipative steel braces to increase both strength and ductility. Steel bracings have some advantages such as their suitability for prefabrication, their relatively low weight, and the possibility to allow inner and outer openings. Moreover, the braces may be directly connected to concrete members without using steel frames fixed to the concrete structure. Ultimately, the use of dissipative braces (such as buckling-restrained axial dampers or steel hysteretic dampers) provides additional benefits in comparison with conventional braces. In fact, they increase the energy dissipation capacity and fix a limitation of the brace force that is transmitted to the highly stressed anchorage. A case study school building was analyzed in this paper. Its capacity was assessed using nonlinear static procedure. A displacement-based procedure was applied for the design of the seismic retrofit, based on the combined use of steel braces and dissipative devices. Nonlinear dynamic time-history analyses were finally performed in order to evaluate the seismic performances and check the effectiveness of the design procedure.

2 SEISMIC RISK OF EXISTING BUILDING

2.1 Geometry, material properties and structural details

The case study deals with a three-storey school building located in Vibo Valentia (Calabria-Italy). The building was designed in 1962 according to the provisions of an Italian Code dating back to 1937 [5]. The site belonged to the first seismic category zone, whose seismic intensity coefficient was C=0.07. The allowable stress design method (also called working stress design method) was used in design. The building consists of three reinforced concrete frame structures (named A, B, and C) (Figure 1a). The elevation view of this structure is shown in Figure 1b. The seismic retrofit was applied to the structure A that has an L-shaped floor plan with dimensions of 17.70 x 35.50 m (Figure 2). All stories have the same height (3.6 m). The cross-sections of the structural members are reported in Table 1. All foundation beams have the same rectangular cross-section 50x100 cm. The floors have a mixed structure made up of reinforced concrete and tiles with a global thickness of 28 cm (25+3 cm). The input data were collected from a variety of sources, including available documentation as well as either in-situ and laboratory measurements or tests. In detail, the following investigations were carried out: 1) geometrical measurements; 2) soil investigations including sampling and testing; 3) determination of mechanical properties of materials by testing of samples taken from the structure. The soil comprises deposits of silt sandy loam, sand slightly silty clay and micaceous sand. The mechanical properties of soil and the ground type according to soil classification of Eurocode 8 [6] were derived from the following geological and geotechnical tests: N.1 soil profile test, N.4 Standard Penetration Tests (SPT), N.2 Dynamic penetrometric tests and N.1 Multichannel Analysis of Surface Waves (MASW) Tests. The synthesis of results from MASW tests gave a value $V_{S,30}$=368 m/s of the propagation velocity of S-waves, $V_{S,30}$ being the average value of propagation velocity of S waves in the upper 30 m of the soil profile. As a consequence, soil was classified as ground type B with $360<V_{S,30}<800$m/s. The building is situated on a flat ground (topographic amplification factor S_T=1.00). In assessing the earthquake resistance of the existing structures, the current Italian Code [7] was applied. For the purpose of choosing the admissible type of analysis and the appropriate confidence factor (CF), the following three knowledge levels are defined in this Code: KL1: Limited knowledge; KL2: Normal knowledge; KL3: Full knowledge. Due to the extensive measuring and testing, in the investigated case study the full knowledge level KL3 may be relied upon (CF=1). The geometry was known from original outline construction drawings integrated by direct visual survey. The structural details were known from original construction drawings together with additional in-situ inspection. Information on the mechanical properties of the construction materials was taken from comprehensive in-situ testing, requiring at least three steel material samples per floor for each type of member and three concrete material samples per floor for every 300 m² of building's total floor area. Collected results gave a mean value of concrete strength f_{cm}=35.2 MPa and a mean value of steel rebars strength f_{ym}=408 MPa.

2.2 Seismic assessment

The seismic performance evaluation was carried out with the procedure reported in both Annex B of EN 1998-3 [6] and current Italian Code [7]. A refined model of the reinforced concrete structure was implemented in the SAP2000 finite element computer program [8]. The assumed values of the live loads are 0.50kN/m² for the top floor and 3.00kN/m² for the other floors. Using the appropriate coefficients from Eurocode 8 [6] the vertical loads were combined with seismic actions in a combination of 1.0G+0.15Q for all the storeys except the top floor, for which the load combination was taken equal to 1.0G+0.30Q. The first three mode shapes of existing building and corresponding dynamic properties are plotted in Figure 3. Table 2 shows the parameters of the elastic design response spectra calculated according to the Italian Code [7].
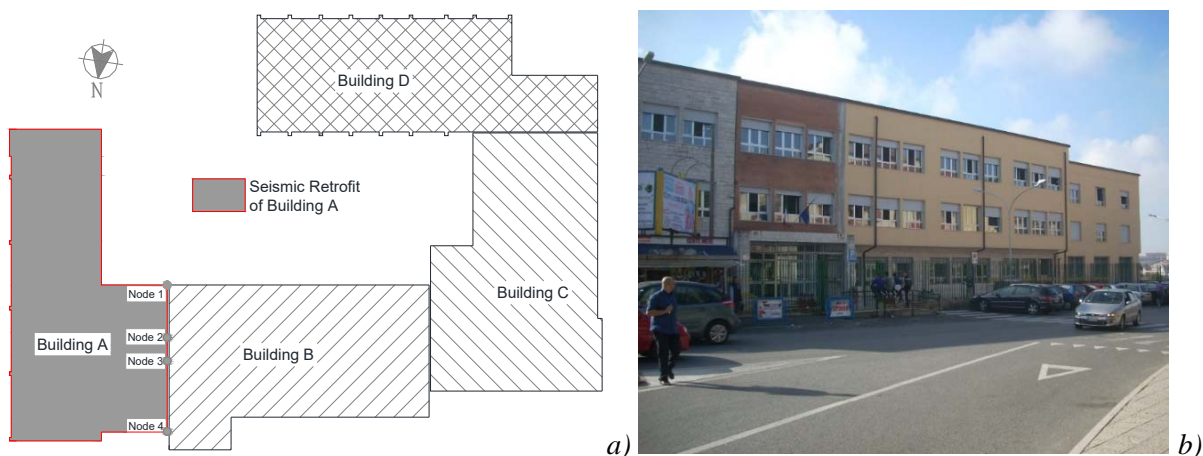
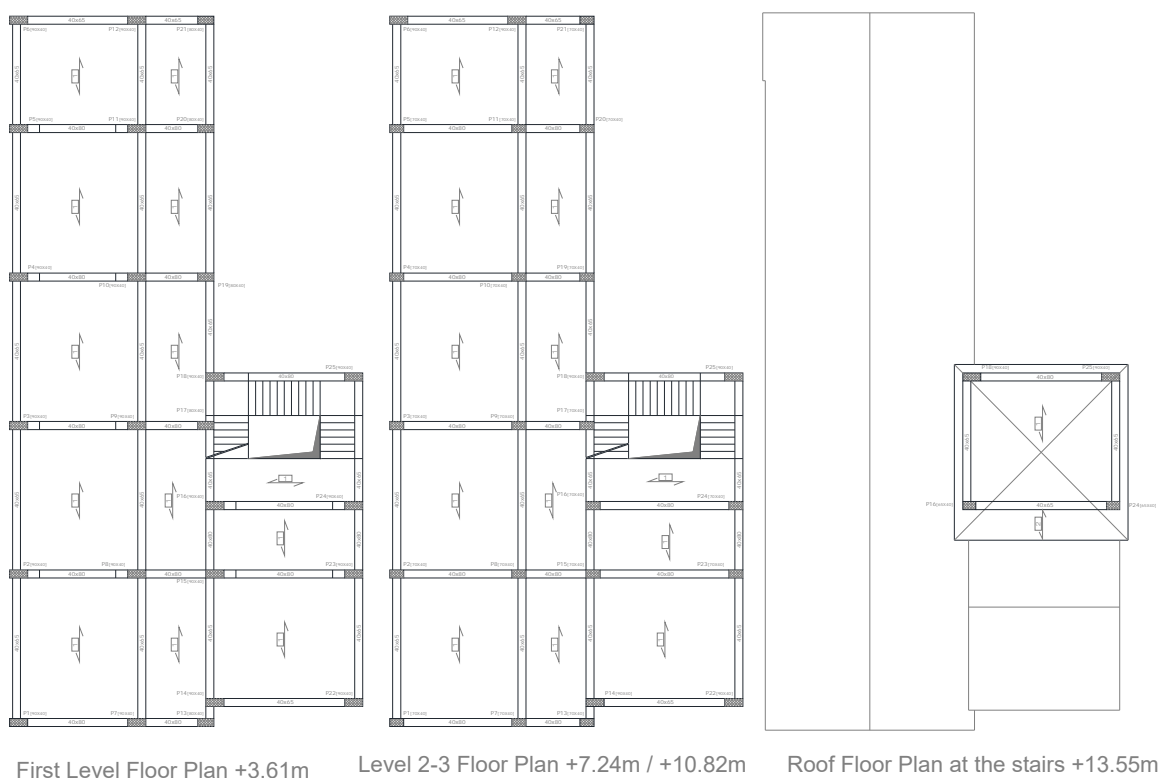Figure 1: a) Plan of the school buildings; b) External view of building A.

First Level Floor Plan +3.61m   Level 2-3 Floor Plan +7.24m / +10.82m   Roof Floor Plan at the stairs +13.55m

Figure 2: Plan views of the investigated section of the school building.

Table 1: Geometry of columns and beams (dimensions in meters).

	COLUMNS			BEAMS	
1st floor	2nd floor	3rd floor	1st floor	2nd floor	3rd floor
0.90 x 0.40	0.90 x 0.40	0.90 x 0.40	0.40 x 0.65	0.40 x 0.65	0.40 x 0.65
0.80 x 0.40	0.70 x 0.40	0.65 x 0.40	0.40 x 0.80	0.40 x 0.80	0.40 x 0.80

Table 2: Parameters of elastic design response spectra (NTC 2008).

Limit State	IO	DL	LS	CP
Probability of exceedance P_{VR}	0.81	0.63	0.10	0.05
Return Period T_R (years)	120	201	1898	2475
Peak ground acceleration PGA/g	0.086	0.112	0.315	0.418
Amplification factor F_o	2.276	2.276	2.448	2.485
Transition Period T_C (s)	0.293	0.315	0.380	0.412

Three performance levels were considered in the analysis. The Limit State (LS) of Damage Limitation (DL) was defined by the chord rotation at yielding, evaluated by the formula (A.10b) of EN 1998-3 [6]. Moreover, the Limit States of Damage Limitation (DL) and Immediate Occupancy (IO) were defined by drift acceptance criteria related to the performance level (0.005 for LS of DL and 2/3x0.005 for LS of IO). The Limit States of Life Safety (LS) was verified by comparison between structural capacity and seismic demand. A nonlinear model based on concentrated plasticity was implemented in the SAP2000 finite element computer program [8]. The plastic hinge model was based on the 3D interaction surface. Plastic hinge generalised load against deformation diagrams used for the modelling were considered bilinear. The stress-strain model originally proposed by Mander *et al.* [9] was used for confined concrete. The steel was modelled with an elastic-plastic-hardening relationship. The rigid elements were placed at beam-column connections to prevent the development of plastic hinges inside the connections. The capacity of ductile and brittle members was estimated in terms of chord rotation and shear strength, respectively. The deformation capacity of beams and columns was defined in terms of the chord rotation. The chord rotation relative to the Limit State (LS) of Life Safety (LS) was assumed as 3/4 of the ultimate chord rotation, evaluated according to the formula A.1 of EN 1998-3 [6]. Figure 4 shows the capacity curves (base shear force vs control node displacement) obtained from nonlinear static (pushover) analysis. The pushover analysis was carried out in two directions (X and Y). Two vertical distributions of the lateral loads were applied: 1) "modal" pattern, consistent with the lateral force distribution determined with the modal analysis; 2) Uniform (rectangular) pattern. The worldwide-assumed code value of ±5% was considered for accidental eccentricity. A large plastic deformation capacity is obtained in Y-direction since the collapse occurs by a global plastic mechanism. On the contrary, the torsional effects in X-direction activate local failure mechanism in many cases, thus limiting the values of displacement ductility capacity. Figure 4 also shows the low shear capacity of brittle components (shear mechanism of beams, columns and joints). For the LS of Life Safety the comparison between capacity and demand was carried out using the procedure implemented in Annex B of EC8 [6] and Italian Code [7]. Table 3 reports the values of the peak ground acceleration (PGA) that represent the capacity of the existing building to resist seismic actions on type A ground for each relevant limit states of the structure (PGA^c_{IO}; PGA^c_{DL}; PGA^c_{LS}). These values were divided by the corresponding reference values (PGA^d) of Table 2, hence giving the risk index ($I_R = PGA^c / PGA^d$) that is given in Table 3.

3   DISPLACEMENT-BASED DESIGN OF DAMPED BRACES

Based on the above analysis, an appropriate retrofit design was set out to overcome the observed deficiencies of the building to resist seismic loads. The main problems can be summarized as: 1) Insufficient stiffness since the damage limitation requirements are not fulfilled (DL and IO Limit States); 2) Poor shear capacity of brittle components (shear mechanism of beams, columns and joints); 3) Torsional effects in X-direction that activate local failure mechanisms; 4) Inadequate member chord rotation capacity (LS Limit State); 5) Inadequate seismic gap from adjacent buildings. The use of concentric steel bracing fitted with dissipative devices was the solution chosen to enhance the earthquake resistance. Steel bracing is easy to implement, cheap and space saving. Also, it effectively combines stiffness, strength and ductility. The steel braces were allocated so to limit the underpinning area of the existing foundation and reduce the torsional effects (Figure 5). Some local member strengthening was applied, including shear retrofit of unconfined joints, fibre reinforced polymer (FRP) shear and bending reinforcement of the first floor beams along the corridor and strengthening of columns adjacent to steel braces by steel angles and strips. Finally, the size of the seismic gap between structures A and B, which was insufficient to avoid structural pounding, had to be increased up to 3 cm. The damped braces were designed according to the

procedure proposed by Mazza et al. [10] following the Displacement-Based Design (DBD) approach. In this context, the lowest capacity curve of the RC bare structure was selected among those corresponding to different lateral-load distributions and accidental eccentricities.

First mode shape
Flexural Y
(α_x=0.03%; α_y=96.88%)
Period 0.681 sec

Second mode shape
Flexural X-Y and Torsional
(α_x=57.93%; α_y=0.22%)
Period 0.485 sec

Third mode shape
Flexural X and Torsional
(α_x=35.16%; α_y=0.09%)
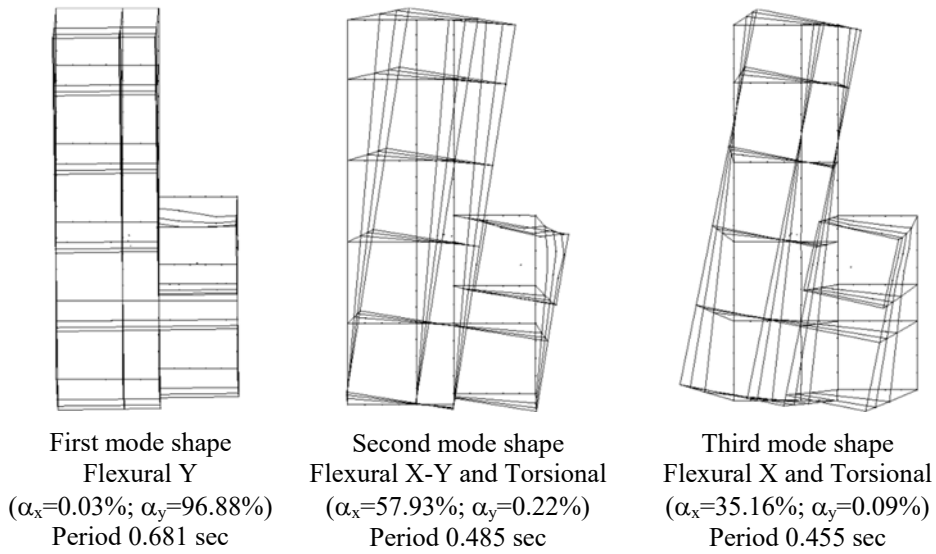Period 0.455 sec

Figure 3: First three mode shapes of the existing building.
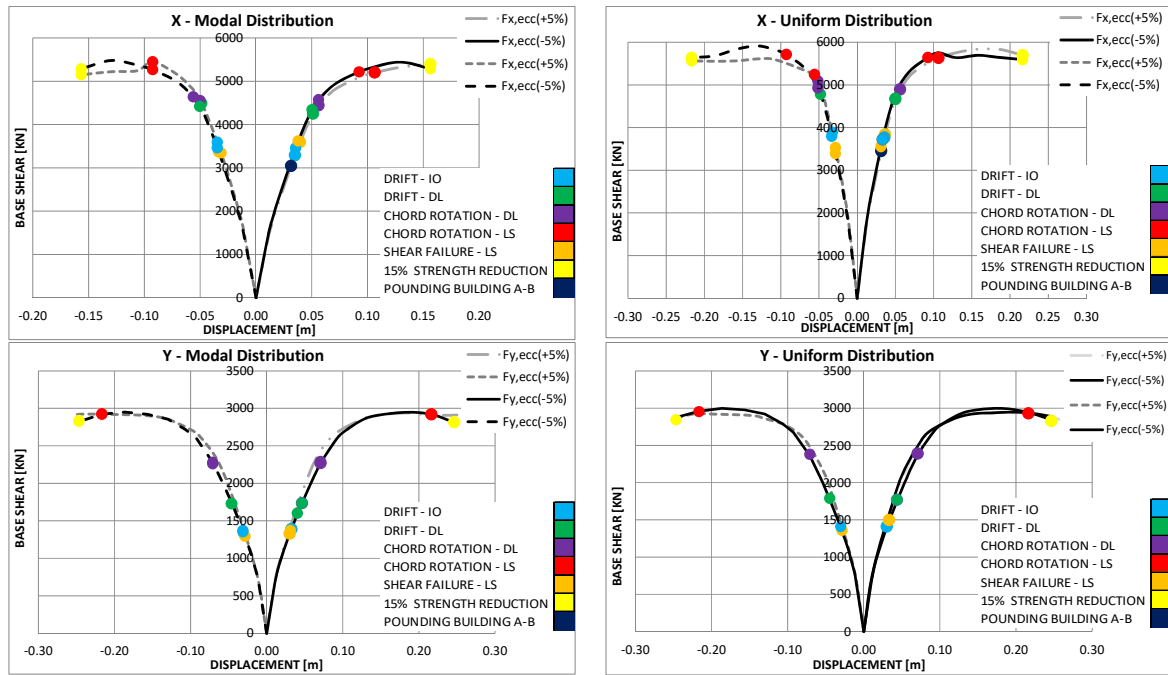

Figure 4: Capacity curves of the existing building.

Table 3: Capacity peak ground acceleration and risk index (IO, DL and LS Limit States).

	IO X-Dir.		DL X-Dir.		LS X-Dir.		IO Y-Dir.		DL Y-Dir.		LS Y-Dir.	
	PGA/g	I_R	PGA/g	I_R	PGA/g	I_R	PGA/g	I_R	PGA/g	I_R	PGA/g	I_R
+Modal + Ecc	0.143	1.402	0.197	1.470	0.351	1.023	0.094	0.922	0.128	0.955	0.432	1.259
- Modal + Ecc	0.151	1.480	0.199	1.485	0.332	0.968	0.090	0.882	0.126	0.940	0.434	1.265
+Modal - Ecc	0.148	1.451	0.197	1.470	0.321	0.936	0.090	0.882	0.126	0.940	0.435	1.268
- Modal - Ecc	0.143	1.402	0.199	1.485	0.325	0.948	0.090	0.882	0.128	0.955	0.431	1.257
+Uniform + Ecc	0.155	1.520	0.204	1.522	0.370	1.079	0.094	0.922	0.128	0.955	0.443	1.292
-Uniform + Ecc	0.152	1.490	0.197	1.470	0.237	0.691	0.090	0.882	0.126	0.940	0.445	1.297
+Uniform - Ecc	0.149	1.461	0.197	1.470	0.340	0.991	0.090	0.882	0.126	0.940	0.446	1.300
-Uniform - Ecc	0.151	1.480	0.202	1.507	0.342	0.997	0.090	0.882	0.126	0.940	0.442	1.289

The selected capacity curve (base shear $V^{(F)}$ vs top displacement $d_p^{(F)}$) was used to define the equivalent bilinear SDOF system according to the formulation proposed by Fajfar [11]. In particular, the design displacement in X-direction ($d_p^{(F)}$=35 mm) was selected in order to avoid seismic pounding with adjacent structure B. In Y-direction the deformability of the unbraced frame is higher and, thus, the design displacement increases. Once the displacement $d_p^{(F)}$ and the corresponding base shear $V_p^{(F)}$ are settled, the yield displacement $d_y^{(F)}$ and stiffness hardening ratio r_F are defined from the capacity curve idealized as bilinear (Figure 6). The equivalent viscous damping due to hysteresis of the RC bare structure was calculated with the Jacobsen formulation [12]. Table 4 shows the parameters of the idealized bilinear SDOF systems for the bare frame (Table 4a) and the damped braces (Table 4b). The equivalent viscous damping of the frame with damped braces (ξ_e) was calculated summing the elastic viscous damping for RC bare framed structure (ξ_v=5%) and the equivalent viscous damping of the system composed of framed structure (F) and damped braces (DB). This damping is evaluated as a weighted average of the equivalent viscous damping factors of bare frame ($\xi^{(F)}$) and dissipative braces ($\xi^{(DB)}$), as follows:

$$\xi_e = \xi_v + \frac{\xi^{(F)}V_p^{(F)} + \xi^{(DB)}V_p^{(DB)}}{V_p^{(F)} + V_p^{(DB)}} \tag{1}$$

The base shear $V_p^{(DB)}$ in dissipative braces is unknown since the effective strength properties of the equivalent damped brace is one of the parameters to be designed. Thus, an iterative procedure is required. At first, the effective period T_e of the framed structure with damped braces is calculated as the period of the the ξ_e-damped displacement spectrum corresponding to the performance displacement d_p.
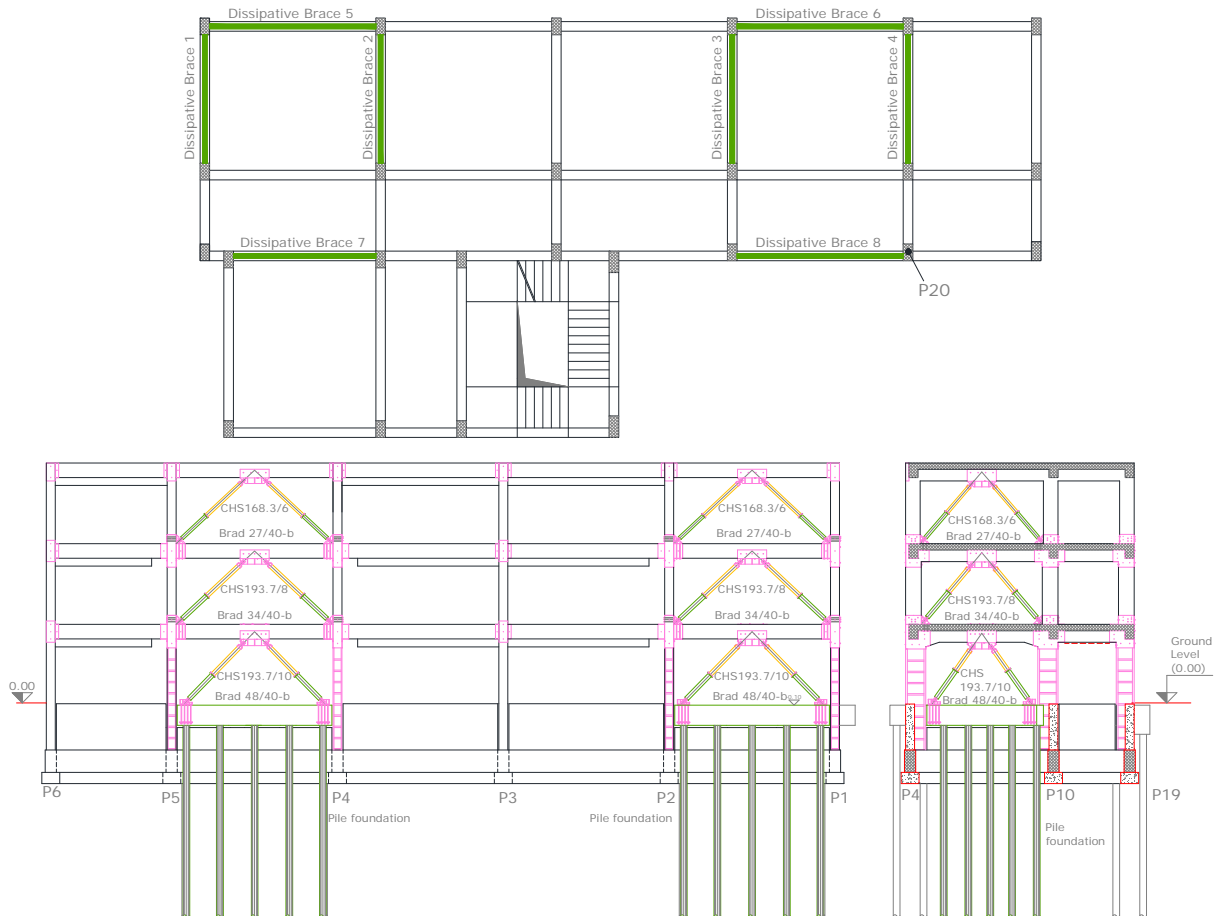

Figure 5: Plan and section view of the school building after retrofit.

Then, the values of the equivalent stiffness, respectively of the frame with damped braces $K_e = 4\pi^2 m_e / T_e^2$ and the damped braces $K_e^{(DB)} = K_e - K_e^{(F)}$ are calculated. Finally, since the constitutive law of the equivalent damped brace are idealized as bilinear, the performance and yielding base shears ($V_p^{(DB)}$ and $V_y^{(DB)}$) are calculated as follows:

$$V_p^{(DB)} = K_e^{(DB)} \cdot d_p; \qquad V_y^{(DB)} = \frac{V_p^{(DB)}}{1 + r_{DB}(\mu_{DB} - 1)} \qquad (2)$$

The base shear from Equation 2 may be used as a new attempt value of $V_p^{(DB)}$ in Equation 1 to calculate the equivalent viscous damping ξ_e of the frame with damped braces. This iterative procedure progresses very quickly to a converged solution. Table 5 shows the parameters of the framed structure with damped braces. According to the proportional stiffness criterion, at each storey the same value of the stiffness ratio between the lateral stiffness values for damped braces and bare frame was assumed. Thus, the mode shapes of the structure may be considered unchanged even after insertion of the damped braces and the base shear may distributed along the height of the building according to the profile corresponding to the fundamental mode (Figure 7). Two different design solutions, one based on buckling-restrained braces (BRB) and one based on steel hysteretic dampers (HBF), were explored (Tables 6-8). Finally, the steel hysteretic dampers were used during the construction phase of the retrofit project (Figure 8).
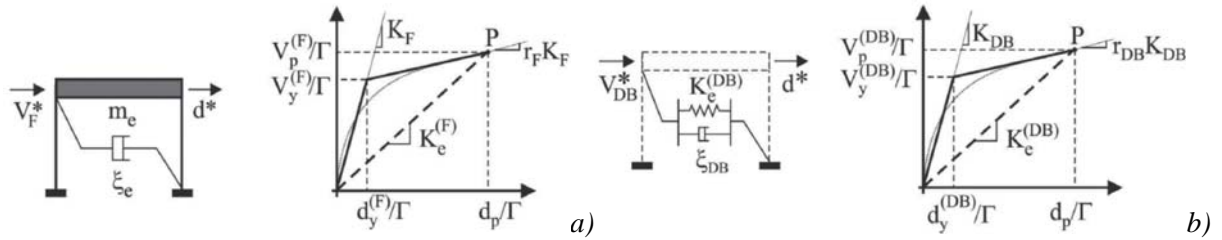

Figure 6: Idealized bilinear SDOF systems: a) Bare frame; b) Damped brace (Mazza et al. [10]).

Table 4: Idealized bilinear SDOF systems: a) Bare frame; b) Damped Brace.

a) SDOF System of bare frame			
Direction	x-x	y-y	
m_e^*	1.138	1.476	kNs^2/mm
Γ	1.417	1.183	-
d_p	50.00	73.85	kNs^2/mm
V_u^F/Γ	3959	2535	kN
V_y^F/Γ	3880	2454	kN
d_u^F/Γ	92	158	mm
d_y^F/Γ	31	62	mm
d_p^*	35.29	62.43	mm
V_p^F*	3886	2454	kN

b) SDOF System of damped braces			
Direction	x-x	y-y	
d_{max}	20	20	mm
r_D	5%	5%	-
d_y	2	2	mm
μ_D	10	10	-
$K_D^* = K_D/K_B < 1$	0.2	0.2	-
$\mu_{DB} = d_p/d_y^{(DB)}$	8.575	8.575	-
r_{DB}	0.06	0.06	-
$\xi_{DB}(\%)$	16%	16%	-

Table 5: Framed structure with damped braces: a) Equivalent SDOF system; b) MDOF system.

a) SDOF System. Bare frame + Damped braces			
Direction	x-x	y-y	
$K_e^{(DB)}$	20.86	24.73	kN/mm
$V_p^{(DB)} = K_e^{(DB)} * d_p$	1043	1826	kN
$V_y^{(DB)} = V_p^{(DB)}/(1 + r_{DB}(\mu_{DB}-1))$	719	1260	kN
ξ_e	9.63%	11.14%	-
R_ξ	0.78	0.73	-
T_D	2.86	2.86	sec
S_{DC}	303	303	mm
T_{eq}	0.61	0.95	sec

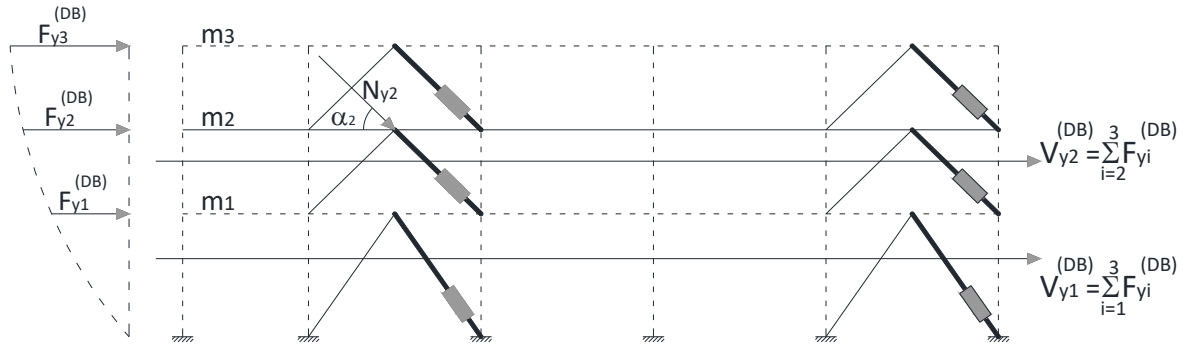| b) MDOF System			
Direction	x-x	y-y	
d_p	50.00	73.9	mm
$K_e^{(DB)}$	20.85	24.73	kN/mn
$V_p^{(DB)} = K_e^{(DB)} \times d_p$	1043	1826	kN
$V_y^{(DB)}$	719	1260	kN
μ_{DB}	8.58	8.58	-
$d_y^{(DB)} = d_p / \mu_{DB}$	5.83	8.61	mm

Figure 7: Distribution of base shear along the height.

Table 6: Seismic design parameters.

			Distribution of base shear along the height									
		Direction x-x						Direction y-y				
Floor	Mass [kNs^2/mm]	Eigen vector [Φ_1]	Brace inclination [α]	F_i [kN]	$V_{y,i}^{(DB)}$ [kN]	$N_{y,i}$ [kN]	$K_i^{(DB)}$ [kN/mm]	Eigen vector [Φ_1]	Brace inclination [α]	F_i [kN]	$V_{y,i}^{(DB)}$ [kN]	$N_{y,i}$ [kN]	$K_i^{(DB)}$ [kN/mm]
1	0.622	0.331	55	136	719	1253	1132.80	0.331	55	136	719	1253	1132.80
2	0.582	0.665	49	256	583	888	694.00	0.665	49	256	583	888	694.00
3	0.429	1.000	49	284	326	497	388.68	1.000	49	284	326	497	388.68

Table 7: Seismic design – Solution 1: Buckling-restrained braces (BRB).

				Distribution of BRB along the height - Direction x-x							
Floor	BRB type	$K_i^{(D)}$ [kN/mm]	L_{BRB} mm	$L_{TOT.}$ mm	L_{Brace} mm	Steel Brace	A_{Brace} [mm^2]	K_{Brace} [kN/mm]	$K_i^{(DB)}$ [kN/mm]	$K_i^{(DB)}{}_{TOT}$ (kN/mm)
1	48/40	210	1640	3400	1760	Φ193.7/10	5770	688.47	160.92	1287.33
2	34/40	153	1625	3660	2035	Φ193.7/8	4670	481.92	116.13	929.04
3	27/40	123	1585	3700	2115	Φ168.3/6	3060	303.83	87.55	700.44

				Distribution of BRB along the height - Direction y-y									
Floor	BRB type	$K_i^{(D)}$ [kN/mm]	L_{BRB} mm	$L_{tot.1}$ mm	$L_{tot.2}$ mm	$L_{Brace\,1}$ mm	$L_{Brace\,2}$ mm	Steel Brace	A_{Brace} [mm^2]	$K_{Brace\,1}$ [kN/mm]	$K_{Brace\,2}$ [kN/mm]	$K_i^{(DB)\,1}$ [kN/mm]	$K_i^{(DB)\,2}$ [kN/mm]	$K_i^{(DB)}{}_{TOT}$ [kN/mm]
1	48/40	210	1640	4220	3911	2580	2271	Φ193.7/10	5770	469.65	533.55	145.11	150.69	1172.06
2	34/40	153	1625	4310	4000	2685	2375	Φ193.7/8	4670	365.25	412.93	107.83	111.64	870.26
3	27/40	123	1585	4310	4000	2725	2415	Φ168.3/6	3060	235.82	266.09	80.84	84.12	653.25

Table 8: Seismic design – Solution 2: Steel Hysteretic Dampers (HBF).

			Distribution of HBF along the height - direction x-x							
Floor	Dissipative Braces	Steel Brace	A_{Brace} [mm^2]	L_{Brace} mm	K_{Brace} [kN/mm]	HBF type	L_{HBF} mm	K_{HBF} [kN/mm]	$L_{tot.}$ mm	$K_i^{(DB)}{}_{TOT}$ (kN/mm)
1	(1-2-3-4)	Φ193.7/20	10908	2.04	1126	420/40	0.58	22.35	2.62	21.915
2	(1-2-3-4)	Φ193.7/14.2	8004	2.29	734	300/40	0.575	15.90	2.87	15.563
3	(1-2-3-4)	Φ168.3/10	4981	2.44	428	240/40	0.575	12.45	3.02	12.098

			Distribution of HBF along the height - direction y-y							
Floor	Dissipative Braces	Steel Brace	A_{Brace} [mm^2]	L_{Brace} mm	K_{Brace} [kN/mm]	HBF type	L_{HBF} mm	K_{HBF} [kN/mm]	$L_{tot.}$ mm	$K_i^{(DB)}{}_{TOT}$ (kN/mm)
1	(5-6-8)	Φ193.7/16	8928	2.71	692	420/40	0.58	22.35	3.29	21.651
2	(5-6-8)	Φ193.7/12.5	7112	2.96	505	300/40	0.575	15.90	3.54	15.414
3	(5-6-8)	Φ168.3/8.8	4407	3.05	304	240/40	0.575	12.45	3.62	11.960
1	(7)	Φ193.7/17.5	9682	2.42	840	420/40	0.58	22.35	3.00	21.771
2	(7)	Φ193.7/12.5	7112	2.66	562	300/40	0.575	15.90	3.23	15.463
3	(7)	Φ168.3/8.8	4407	2.73	339	240/40	0.575	12.45	3.31	12.009

Figure 8: The building after retrofit: a) External view. b) Detail of braces fitted with hysteretic dampers.

4 SEISMIC BEHAVIOUR OF THE RETROFITTED STRUCTURE

Hysteretic devices arranged within steel braces were used as structural fuses and designed according to capacity design. Thus, the capacity of braces is never exceeded, so avoiding local instability. A refined model of the school building after retrofit was implemented in the SAP2000 code [8] (Figure 9). The first three mode shapes of retrofitted building and corresponding dynamic properties are shown in Figure 10. It can be observed that the steel bracing is effective in reducing the torsional effects. In fact, while in the existing structure a flexural X-Y and torsional second mode shape are obtained (Figure 3), the retrofitted structure shows a flexural X second mode shape with an effective modal mass greater than 85% (Figure 10).

According to recent seismic codes, two methods are available to study the inelastic response of the structure: a) Nonlinear Static (Pushover) Analysis; b) Nonlinear Response History Analysis. The dissipative braces were modelled with an in-series model composed by an elastic steel brace and a hysteretic bilinear damper. Two vertical distributions of the lateral loads were considered in the pushover analysis: 1) First Mode: acceleration profile corresponding to the fundamental mode; 2) Uniform (rectangular). In Figure 11 the pushover curves obtained before and after retrofit are compared. Results show that the dissipative steel bracing is successful in increasing the stiffness, strength and ductility of the bare structure. The seismic performance can be evaluated with the code procedure [6-7], that is equivalent to the capacity spectrum method based on inelastic demand spectra [11]. The Elastic Demand Response Spectrum (EDRS) is generally represented by the 5%-damped response spectrum. However, in the case under exam the application of this procedure might be too much conservative. In fact, the hysteretic steel dampers are characterized by a very low yield displacement (2 mm). Thus, their energy dissipation during earthquake ground motion is very high and it could be not properly represented by the comparison between pushover curve and 5%-damped response spectrum.
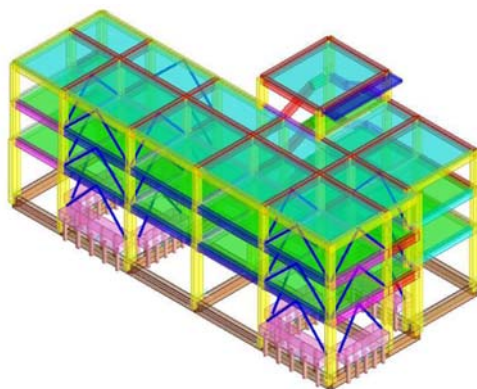

Figure 9: Three-dimensional finite element model of the investigated school building.

First mode shape
Flexural Y
(α_x=0.77%; α_y=86.57%)
Period 0.433 sec

Second mode shape
Flexural X
(α_x=85.18%; α_y=2.43%)
Period 0.393 sec

Third mode shape
Torsional
(α_x=6.59%; α_y=5.77%)
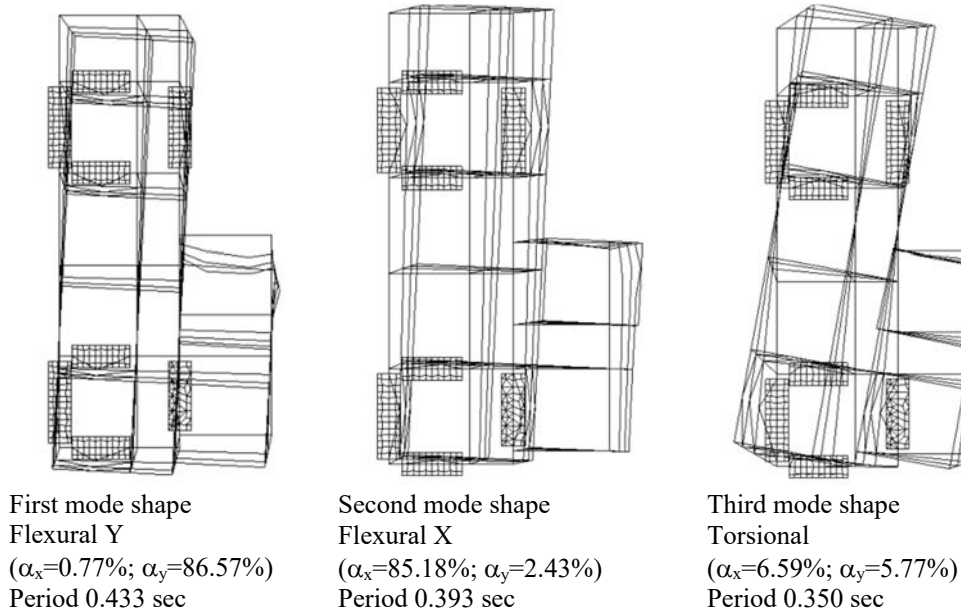Period 0.350 sec

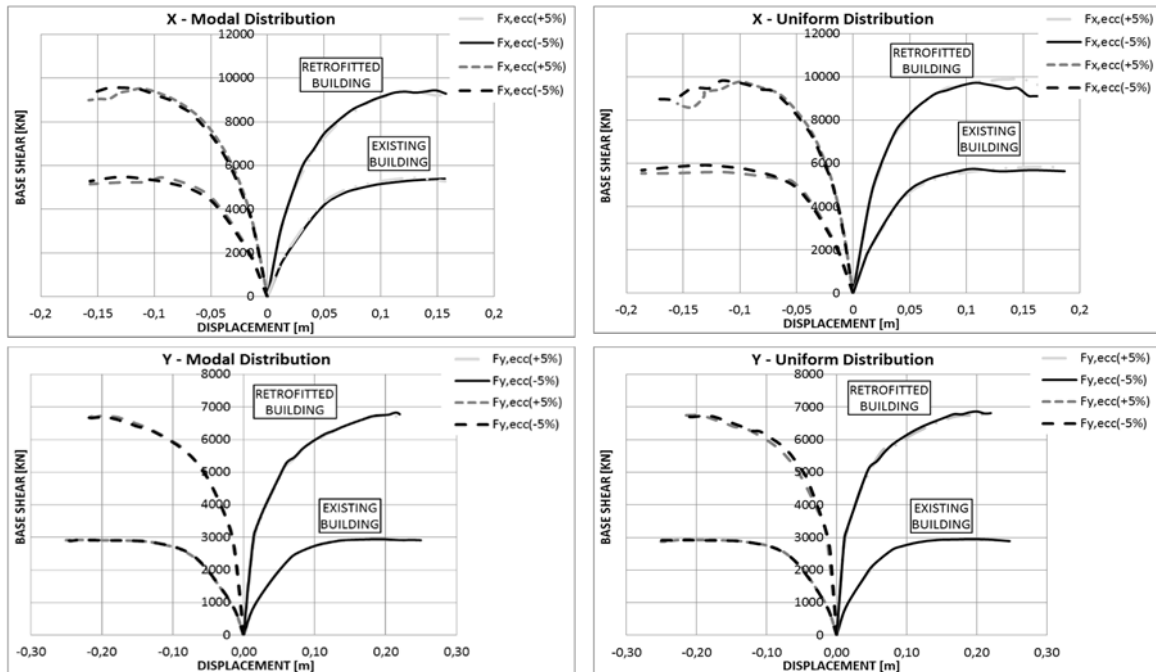Figure 10: First three mode shapes of building after retrofit.

Figure 11: Capacity curves. Comparison between existing and retrofitted building.

On the other side, the equivalent linearization procedures in literature [13] require the definition of the appropriate level of effective damping and, thus, they may lead to an overestimation of the damping due to hysteresis [14]. Thus, in this paper the seismic assessment was carried out by direct numerical integration of the equations of motion. The constitutive law of the hysteretic steel dampers was approximated by the well-known Bouc-Wen model. The seismic motion consisted of two simultaneously acting accelerograms along both horizontal directions. A group of 3 pairs of time-histories was applied for Life Safety and Collapse Prevention Limit States. The envelope of the response quantities from all the analyses was used as the design value of the seismic effect. The description of the seismic motion was made by using artificial accelerograms [15]. The choice of accelerograms followed the rules recommended in the seismic standards [7]. At the Life Safety Performance Level, member chord rotation demand

of primary ductile elements was compared to the corresponding envelope chord rotation capacity. For beams the demand in terms of chord rotation was obtained as the envelope of peak values obtained for each pairs of time-histories and then compared to chord rotation capacity. For columns, the effects of biaxial bending should be considered. In Figure 12a the comparison between capacity and demand in terms of chord rotation of column P20 (see Figure 5) is plotted. The time-history of chord rotation always lies within the straight lines that bound the safe domain. These lines were obtained as follows. The chord rotation is defined as the angle between the tangent to the member axis at the end section and the chord connecting the centroid of the end section of the member and the centroid of the section at which $M=0$ (point of contraflexure). Thus, each column is considered as formed by two cantilevers fixed at the member ends, with a length equal to the shear span length $L_s=M/V$. In columns under seismic ground motion the nodal rotation is low with respect to the drift Δ of the equivalent cantilever (that is the chord rotation θ may be reasonably defined as $\theta=\Delta/L_s$). In the same way, the point of contraflexure may be considered placed at the middle of the column, that is $L_s=L/2$ where L is the length of the column. Thus, the chord rotation capacity θ_{LS} at the Life Safety LS immediately gives the corresponding drift $\Delta_{LS}=\theta_{LS}L/2$. Considering the bi-axial bending, the drift capacity at the Life Safety LS depend on the direction of bending axle. In this paper, the limit domain is defined under the hypothesis of linear variation between the values obtained in the case of pure X- and Y- bending (Figure 12a). In Figure 12b the X- and Y- displacement time-histories of node 1 (see Figure 1) are plotted. In the same graph, the minimum seismic gap (3 cm) to avoid pounding between structures A and B is shown. Results evidence that the risk of pounding between adjacent structures during strong earthquakes is avoided. In Figure 13, the hysteresis loops of some steel dampers under at the Collapse Prevention LS are plotted. Results also show that steel dampers at the third level remain elastic.
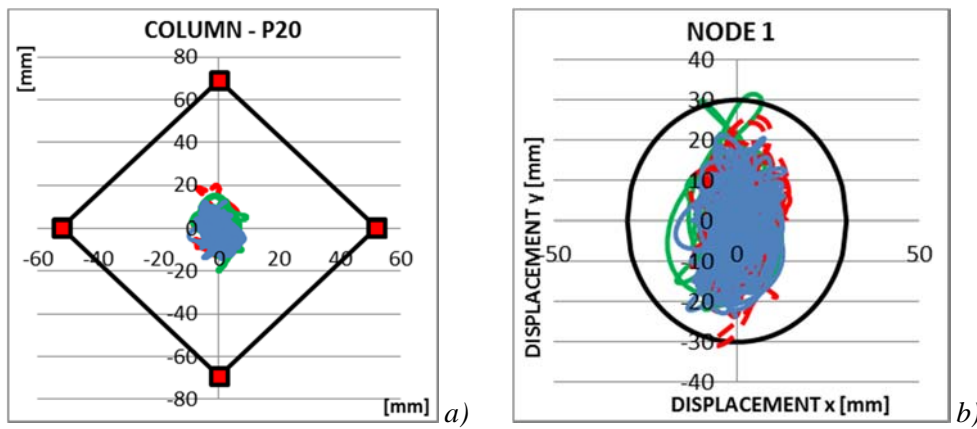

Figure 12: a) Interstorey drift time-history at column P20; b) X-Y displacement time-history of node 1.
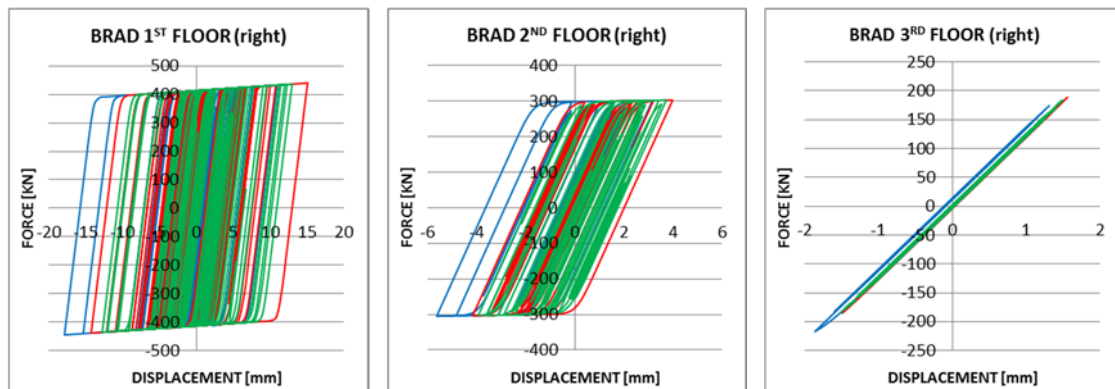

Figure 13: Hysteresis loops of steel dampers at 1st, 2nd and 3rd floor.

5 CONCLUSIONS

The paper illustrates the analysis and design of a RC school building retrofitted with steel braces and hysteretic dampers. The retrofitting design and construction were described in detail. Results evidenced that the retrofit with dissipative steel braces was effective in increasing the energy dissipation capacity even with low lateral displacement demand. This is a very important feature for existing structures, which have low ductility capacity and high seismic hazard of pounding during earthquake excitation. The results from nonlinear time history analysis show that the displacement-based design procedure is effective in ensuring the safety both of structure at the Life Safety Limit State and of damped braces at the Collapse Prevention Limit State. However, it should be observed that the hysteretic steel dampers of the third level remain elastic under earthquake ground motion. Thus, the design procedure could be improved with a parameter optimization that can potentially improve dampers performance.

REFERENCES

[1] Ferraioli M. and Mandara A., "Base Isolation for Seismic Retrofitting of a Multiple Building Structure: Design, Construction, and Assessment", *Mathematical Problems in Engineering*, 1-24, 2017.

[2] Ferraioli M. and Mandara A., "Base Isolation for Seismic Retrofitting of a Multiple Building Structure: Evaluation of Equivalent Linearization Method", *Mathematical Problems in Engineering*, 1-17, 2016.

[3] Ferraioli M., "Case study of seismic performance assessment of irregular RC buildings: hospital structure of Avezzano (L'Aquila, Italy)", *Earthquake Engineering and Engineering Vibration*, **14**, 141-156, 2015.

[4] Ferraioli M., Abruzzese D., Miccoli L., Vari A. and Di Lauro G., "Structural identification from environmental vibration testing of an asymmetric-plan hospital building in Italy", *Proc. of Int. Conference Urban Habitat Constructions under catastrophic events*, Napoli, **1**, 981-986, 2010.

[5] Royal Decree n. 2105, 22/11/1937, *Norme tecniche ed igieniche per le riparazioni, le ricostruzioni e nuove costruzioni degli edifici pubblici e privati nei comuni o frazioni di comune dichiarati zone sismiche (Regulations for seismic design and retrofit of buildings)*. GU n.298, Rome. (in Italian).

[6] Comité Européen de Normalisation CEN, *EN1998 - Eurocode 8: Design provisions for earthquake resistance of structures*, European Communities for Standardization, Brussels, Belgium, 2004.

[7] NTC 2008, *Norme Tecniche per le Costruzioni*, D.M. Infrastrutture Trasporti 14 gennaio 2008.

[8] CSI Computer & Structures Inc. SAP2000, *Linear and nonlinear static and dynamic analysis of three-dimensional structures*, Berkeley (CA), C.E., 2015.

[9] Mander J.B., Priestley M.J.N. and Park R., "Theoretical stress-strain model for confined concrete", *Journal of Structural Engineering*, **114** (8), pp.1804–1826, 1988.

[10] Mazza F. and Vulcano A. "Design of hysteretic damped braces to improve the seismic performance of steel and RC framed structures", *Ingegneria Sismica,* **31**(1):5–16, 2014.

[11] Fajfar P., "Capacity spectrum method based on inelastic demand spectra", *Earthquake Engineering Structural Dynamics*, **28**, 979-993, 1999.

[12] Jacobsen L.S. "Steady forced vibrations as influenced by damping," *ASME Transaction* **52** (1), 69-181, 1930.

[13] FEMA, *Improvement of nonlinear static seismic analysis procedures*, prepared by the Applied Technology Council (ATC-55 Project), FEMA 440, published by the Federal Emergency Management Agency, Washington, 2005.

[14] Ferraioli M., Lavino A., Avossa A.M. and Mandara A., "Evaluation of nonlinear static procedures for seismic performance assessment of BRBF structures", *Proceedings of 7th International Conference on Behaviour of Steel Structures in Seismic Areas (STESSA),* Santiago, Chile, 2012.

[15] SIMQKE, *User Manual*, Nisee Software Library, University of California, Berkeley, USA, 1976.